

MIT Open Access Articles

A simplified description of the evolution of organic aerosol composition in the atmosphere

The MIT Faculty has made this article openly available. **Please share** how this access benefits you. Your story matters.

Citation: Heald, C. L., J. H. Kroll, J. L. Jimenez, K. S. Docherty, P. F. DeCarlo, A. C. Aiken, Q. Chen, S. T. Martin, D. K. Farmer, and P. Artaxo (2010), A simplified description of the evolution of organic aerosol composition in the atmosphere, *Geophys. Res. Lett.*, 37, L08803, doi:10.1029/2010GL042737. ©2010 American Geophysical Union

As Published: <http://dx.doi.org/10.1029/2010GL042737>

Publisher: American Geophysical Union

Persistent URL: <http://hdl.handle.net/1721.1/60917>

Version: Author's final manuscript: final author's manuscript post peer review, without publisher's formatting or copy editing

Terms of use: Attribution-Noncommercial-Share Alike 3.0



1 **A simplified description of the evolution of organic aerosol composition in the atmosphere**

2 C. L. Heald^{1§*}, J. H. Kroll^{2§}, J. L. Jimenez³, K. S. Docherty³, P. F. DeCarlo^{4,5}, A. C. Aiken^{3,6}, Q. Chen⁷,
3 S.T. Martin⁷, D. K. Farmer³, P. Artaxo⁸

4
5 ¹ *Dept of Atmospheric Science, Colorado State University, Fort Collins, CO, USA*

6 ² *Dept of Civil and Environmental Engineering, Massachusetts Institute of Technology, Cambridge, MA,*
7 *USA*

8 ³ *CIRES and Dept of Chemistry and Biochemistry, University of Colorado, Boulder, CO, USA*

9 ⁴ *CIRES and Dept of Atmospheric and Oceanic Sciences, University of Colorado, Boulder, CO, USA*

10 ⁵ *now at Paul Scherrer Institute, Villigen, Switzerland*

11 ⁶ *now at ETH, Zurich, Switzerland*

12 ⁷ *School of Engineering and Applied Sciences & Dept of Earth and Planetary Sciences, Harvard*
13 *University, Cambridge, MA, USA*

14 ⁸ *University of Sao Paulo, Sao Paulo, Brazil*

15 [§] *Authors contributed equally to this work.*

16 ^{*} *Corresponding author (heald@atmos.colosate.edu)*

17

18

19

20 **ABSTRACT**

21 Organic aerosol (OA) in the atmosphere consists of a multitude of organic species which are either
22 directly emitted or the products of a variety of chemical reactions. This complexity challenges our ability
23 to explicitly characterize the chemical composition of these particles. We find that the bulk composition
24 of OA from a variety of environments (laboratory and field) occupies a narrow range in the space of a
25 Van Krevelen diagram (H:C versus O:C), characterized by a slope of ~ -1 . The data show that
26 atmospheric aging, involving processes such as volatilization, oxidation, mixing of air masses or
27 condensation of further products, is consistent with movement along this line, producing a more oxidized
28 aerosol. This finding has implications for our understanding of the evolution of atmospheric OA and
29 representation of these processes in models.

30

31 INTRODUCTION

32 Organic aerosol (OA) makes up an important, sometimes dominant, fraction of submicron particulate
33 matter in the atmosphere [Zhang *et al.*, 2007]. However, models are generally unsuccessful in
34 reproducing the observed magnitudes and variability of these particles [Capes *et al.*, 2009; de Gouw *et al.*,
35 2005; Heald *et al.*, 2005; Heald *et al.*, 2006; Johnson *et al.*, 2006; Kleinman *et al.*, 2008; Volkamer *et al.*,
36 2006]. Such difficulties likely arise from complexity in the sources (including both primary combustion
37 emissions, POA, and secondary production SOA), composition, and chemistry of OA. While traditionally
38 SOA has been thought to consist of products from a few classes of compounds (terpenes and aromatics),
39 recent studies have identified both additional precursors [Kroll *et al.*, 2005; Lim and Ziemann, 2009;
40 Robinson *et al.*, 2007; Volkamer *et al.*, 2009] and additional formation pathways [Carlton *et al.*, 2007;
41 Kalberer *et al.*, 2004]. Once formed in the atmosphere, the pool of OA remains dynamic, through both
42 reversible partitioning and continued atmospheric oxidation. This additional processing (“aging”) is
43 generally not well-represented in models as it involves a number of physical and chemical processes that
44 are typically not accessed in laboratory experiments. Furthermore, air mass mixing in the atmosphere
45 implies a blending of OA from various sources. In this study, we identify compositional characteristics
46 shared by atmospheric OA formed under a wide range of reaction conditions (different environments,
47 precursors, volatilities, and photochemical ages) using a Van Krevelen diagram.

48

49

50 THE VAN KREVELEN DIAGRAM

51 The Van Krevelen diagram was developed to illustrate how elemental composition changes during coal
52 formation [Van Krevelen, 1950]. The diagram cross plots the hydrogen to carbon atomic ratio (H:C) and
53 the oxygen to carbon atomic ratio (O:C). It has seen recent use for the graphical interpretation of ultra-
54 high resolution mass spectrometric data, in which the elemental ratios of individual compounds are
55 plotted instead of those of the bulk material [Kim *et al.*, 2003]. This approach has recently been applied

56 towards the mass spectrometric measurement of individual species within atmospheric OA (e.g. [Bateman
57 *et al.*, 2009]), but to our knowledge has not been used for bulk aerosol measurements.

58
59 Figure 1 shows a conceptual Van Krevelen diagram for organic material in the atmosphere, where the
60 most oxidized species lie at the lower right. This space can be used to illustrate how reactions involving
61 the addition of functional groups fall along straight lines. For example, the replacement of an aliphatic
62 carbon (-CH₂-) with a carbonyl group (-C(=O)-) implies a loss of 2 hydrogens and a gain of 1 oxygen, and
63 thus a slope of -2 in the Van Krevelen diagram. Conversely, the replacement of a hydrogen with an
64 alcohol group (-OH) involves an increase in oxygen but no change in hydrogen, and therefore is a
65 horizontal line in Van Krevelen space. An intermediate slope of -1 is produced by the simultaneous
66 addition of both functional groups, forming a hydroxycarbonyl or carboxylic acid. Organic atmospheric
67 functionalization reactions, including, but not limited to those shown here, generally involve changes not
68 only to O:C but also to H:C. While increasing O:C is often considered an indicator of atmospheric
69 oxidation (e.g. [DeCarlo *et al.*, 2008]), Figure 1 shows that a non-oxidative process such as hydration
70 reactions can be misinterpreted based on this limited description. Conversely, the oxidation of an alcohol
71 to a carbonyl involves no change to O:C.

72 73 **APPLICATION OF THE VAN KREVELEN DIAGRAM TO ATMOSPHERIC AEROSOL**

74 Atmospheric OA consists of a multitude of compounds with a wide range of properties. Typically less
75 than 20% of the mass of OA can be speciated [Williams *et al.*, 2007]. Estimation of bulk elemental ratios
76 can provide insight into the composition of OA in the atmosphere. One recently used method utilizes data
77 from the Aerodyne high resolution aerosol mass spectrometer (HR-AMS). The HR-AMS provides mass
78 spectra of an ensemble of submicron OA particles in real time, with sufficiently high mass resolution that
79 the chemical formulae of all important ions (especially below $m/z \leq 100$) can be unambiguously
80 determined [DeCarlo *et al.*, 2006]. As demonstrated by Aiken *et al.* [2007; 2008], summation of the

81 abundances of each element within each ion, and correction by an empirical factor to account for biases in
82 ion fragmentation, allows for the determination of elemental ratios (O:C and H:C) of the OA. Results for
83 individual organics are somewhat uncertain (with errors of ~30% for O:C and 10% for H:C [Aiken *et al.*,
84 2007]), but these uncertainties are likely to be substantially lower for the large ensemble of organics
85 found in ambient aerosol, due to averaging of non-systematic errors. Elemental ratios estimated from
86 AMS measurements from several laboratory and field measurements are explored here.

87
88 Figure 2 shows a Van Krevelen diagram of the bulk composition of OA. Mean values from field
89 experiments are shown as solid circles. These include the Study of Organic Aerosol at Riverside (SOAR-
90 1) campaign in Riverside, California in summer 2005, the Amazonian Aerosol Characterization
91 Experiment (AMAZE-08) in the central Amazon Basin, during the wet season of 2008 [Chen *et al.*,
92 2009], and both the aircraft and T0 site during the Megacity Initiative: Local and Global Research
93 Observations (MILAGRO) campaign in Mexico City in Spring 2006 [Aiken *et al.*, 2008; DeCarlo *et al.*,
94 2008]. Also shown is the elemental composition of the individual Positive Matrix Factorization factors
95 during MILAGRO. These factors have been shown to represent freshly emitted OA (HOA, BBOA) and
96 more oxidized OA (progressing from OOA2 to “aged” OOA1) [Aiken *et al.*, 2008]. Laboratory studies
97 are shown with diamonds. These include a series of vehicle and biomass burning POA (diesel, gasoline,
98 smoke from lodgepole pine and sage/rabbitbrush burning) from Aiken *et al.* [2008], laboratory-generated
99 SOA from α -pinene ozonolysis at decreasing OA mass loadings (from left to right) [Shilling *et al.*, 2009]
100 and the products of heterogeneous oxidation of squalane with increasing OH exposure (from left to right)
101 [Kroll *et al.*, 2009]. Finally, the evolution of the elemental composition of OA for a series of thermo-
102 denuder experiments (with temperature increasing left to right) is shown as open circles [Huffman *et al.*,
103 2009]. All these data line up in the Van Krevelen diagram along a line with a slope of ~ -1 .

104

105 Figure 3 shows the Van Krevelen diagrams for the complete set of OA measurements from three field
106 campaigns (SOAR-1, AMAZE-08, and MILAGRO) where measurements line up approximately with the
107 -1 slope (slopes of -1.1, -1.1, 0.8 fitted with reduced-major axis approach) with Pearson correlation
108 coefficients of -0.90, -0.64 and -0.62 respectively. The aerosols sampled at Riverside exhibit a limited
109 range of composition, which likely reflects predominantly anthropogenic sources of OA, both primary
110 and secondary, transported from the center of the Los Angeles basin. Aerosol loadings at the AMAZE-08
111 site, are substantially lower [Chen *et al.*, 2009] which may explain the higher degree of scatter on the
112 elemental ratios. OA in this clean, forested environment exhibits a wide range of oxygen content, with
113 more oxidized aerosol than observed at Riverside. This may be the result of differences in aerosol
114 sources, level of aging, and/or aerosol loading. Given the more extensive sampling of source types and air
115 mass ages possible aboard an aircraft compared to a single field site, the observations made aboard the C-
116 130 during the MILAGRO campaign likely reflect the most diverse dataset here. These measurements are
117 colored by a photochemical clock representing the conversion of nitrogen oxides to total reactive
118 nitrogen. We find that the aerosol composition generally appears to move down this composition line in
119 Van Krevelen space, as a function of photochemical age.

120

121

122 **DISCUSSION**

123 Figures 2 and 3 illustrate that OA occupies a remarkably narrow linear area in Van Krevelen space,
124 indicating a tight coupling between particulate H:C and O:C. Thus OA has a characteristic bulk elemental
125 composition, with a rough empirical formula of $\text{CH}_{2-x}\text{O}_x$ ($x=0-1$). This holds true for a wide range of OA
126 types - laboratory/ambient, biogenic/anthropogenic, urban/remote, and freshly emitted/aged. It should be
127 emphasized that since Van Krevelen plots provide no information on molecular structure or carbon
128 number, the molecular species in each case are almost certainly different, even if the average elemental
129 compositions are the same. Moreover, all reported elemental ratios are bulk measurements, the averages

130 of a very large number of different molecules, and individual species have a much wider range of H:C
131 and O:C. Indeed, ultrahigh-resolution electrospray ionization mass spectrometry of SOA (e.g., [Bateman
132 *et al.*, 2009]) results in Van Krevelen plots that are roughly centered on the fitted line, but with a good
133 deal of spread in both the H:C and O:C dimensions. At the same time, the fact that aerosol sampled at
134 different loadings [Shilling *et al.*, 2009] and temperatures [Huffman *et al.*, 2009] fall along the same line
135 indicates that aerosol components of different volatilities do not deviate substantially from this general
136 elemental composition trend, and that volatilization processes involve movement along this line.

137
138 As oxidation involves movement towards the right (higher O:C) and the bottom (lower H:C) of the Van
139 Krevelen diagram (Figure 1), the data in Figures 2 and 3 span a range of oxidation of the OA. The
140 trajectory defined by the fitted line in the Van Krevelen diagram can represent some combination of
141 physical mixing and aerosol aging (oxidation, volatilization, condensation). While these processes are
142 inextricable for field studies, the laboratory results [Huffman *et al.*, 2009; Kroll *et al.*, 2009; Shilling *et*
143 *al.*, 2009] shown in Figure 2 strongly suggest that the fitted line defines an average elemental trajectory
144 associated with aerosol aging. The slope of -1 indicates that for each oxygen atom added upon oxidation,
145 a hydrogen atom is lost. This change is consistent with equal increases in carbonyl and alcohol moieties,
146 such as carboxylic acid addition (Figure 1) as well as with the observed increase in the intensity of the m/z
147 44 ion (thought to be a marker of acid groups in AMS measurements [Aiken *et al.*, 2008]).

148
149 Ambient measurements also scatter around the -1 slope in the Van Krevelen diagram. In particular, the
150 MILAGRO measurements of OA at different photochemical ages suggest a trajectory towards more
151 oxidized aerosol with time (Figure 3c), Physical mixing of fresh POA (O:C~0, H:C~2) with more
152 oxygenated OA (O:C~0.5, H:C~1.5) can generate the observed -1 slope, but is likely to play a role only in
153 close proximity to emission sources. This may contribute to the strong correlation observed at the
154 Riverside site (Figure 3a).

155

156 This general relationship related to the elemental composition of the aerosol can be used to assess the
157 potential importance of individual species or processes. For example, given that isoprene tetrols
158 (O:C=0.8, H:C=2.4) or glyoxal oligomers (which involves the addition of two water molecules, such that
159 O:C=1.25-2 and H:C=1.5-3 for n=1-4) lie substantially above the line in Figures 2-3, their presence
160 would need to be balanced by compounds with low H:C and O:C, suggesting that they do not make up a
161 major fraction of mass of the aerosol studied. Similarly, hydration/dehydration reactions sometimes
162 associated with oligomerization reactions of particulate organics, involve movement in Van Krevelen
163 space inconsistent with observations, suggesting they do not dominate the evolution of atmospheric
164 aerosol.

165

166 It should be noted that the slope or intercept of the best-fit line for some individual datasets is somewhat
167 different than that shown in Figure 2. The line originates at O:C = 0 and H:C = 2, corresponding to an
168 alkene or cycloalkane (or arbitrarily long acyclic alkane). However, some of the individual data sets
169 shown, while exhibiting a slope of ~ -1 , have a somewhat lower y-intercept; examples include the two
170 datasets of SOA from α -pinene ozonolysis [Huffman *et al.*, 2009; Shilling *et al.*, 2009] as well as the
171 AMAZE-08 observations (from a site heavily influenced by isoprene chemistry). Such differences may
172 result from the fact that the SOA precursors fall well below the fitted line ($H:C_{\text{terpene}}=1.6$). However, the
173 y-intercepts (~ 1.8) are not quite as low, indicating that the formation of condensable products involved
174 the addition of O with no loss (and possibly a gain) of H, in accordance with known mechanisms [Calvert
175 *et al.*, 2000]. The same is also likely to hold true for SOA from other polyunsaturated species, such as
176 aromatic hydrocarbons (e.g. $H:C_{\text{toluene}}=1.14$). Moreover, the interpretation of the aerosol composition as a
177 pure H-C-O system does not account for nitrogen or sulfur containing moieties. These might influence
178 measured O:C or H:C, and may in fact explain some of the scatter observed in the measurements made in
179 urban/polluted areas (Figure 3).

180

181 While the dominant compositional changes observed proceed along a ~ -1 slope, this tight compositional
182 relationship does not hold for all of the datasets. Much of the MILAGRO data (Figure 3c) follows the -1
183 slope but levels off at high oxidation levels (reducing the overall fitted slope to -0.8). The heterogeneous
184 oxidation of squalane (green diamonds in Figure 2) shows a similar shallow slope at high O:C. This may
185 suggest the greater tendency for alcohol addition, or the increased importance of C-C bond breaking
186 (fragmentation) reactions, which lead to relatively small changes in H:C. For example, if a carboxylic
187 acid group is added to the site of a C-C bond cleavage, as suggested by recent experimental work [*Kroll et*
188 *al.*, 2009], the net effect would be to replace a $-\text{CH}_2-$ group with a $-\text{COOH}$ group, for a slope of only $-$
189 $1/2$. The composition trend in squalane oxidation in fact appears never to follow the -1 slope. This may
190 represent a contrast between a single-compound experiment vs a complex atmospheric system where the
191 multiplicity of molecular structures and oxidation pathways average out variability. Further studies of
192 multigenerational oxidative processing are necessary to better understand how the abundances of
193 individual functional groups change upon aging or volatilization in the atmosphere.

194

195 **CONCLUSIONS**

196 The development of accurate models of OA processing in the atmosphere has been stymied by both a
197 paucity of laboratory constraints on these processes, and the computational cost implicit in a detailed
198 chemical description of these reactions. Atmospheric OA is shown here to have a narrow range of bulk
199 elemental composition, despite the large diversity of constituent molecules. H:C and O:C of a wide range
200 of aerosol types are related linearly, with a ~ -1 slope in Van Krevelen space. Volatilization and oxidative
201 aging, two key physical and chemical processes that OA is subject to after emission or formation, both
202 involve movement along this line, resulting in a more oxidized aerosol. Mixing of fresh and aged air
203 masses may also produce a similar OA trajectory. These results suggest that the chemical evolution of OA
204 in the atmosphere may be simply represented in models. Development of a generalized scheme requires

205 further investigation of the time scales for this aging in different environments. A complete description of
206 OA processing must link these compositional changes with key physical properties (e.g. volatility,
207 hygroscopicity, light absorption) of the aerosol.

208

209

210 **ACKNOWLEDGMENTS**

211 This work was supported in part by NSF grants ATM-0929282, ATM-0449815, and ATM-0723582 and
212 NOAA grant NA08OAR4310565. We thank A. J. Weinheimer (NCAR) for providing the MILAGRO
213 NO_x/NO_y observations.

214 **REFERENCES**

215

216 Aiken, A. C., et al. (2007), Elemental Analysis of Organic Species with Electron Ionization High-
217 Resolution Mass Spectrometry, *Anal. Chem.*, *79*, 8350-8358.

218 Aiken, A. C., et al. (2008), O/C and OM/OC ratios of primary, secondary, and ambient organic aerosols
219 with high-resolution time-of-flight aerosol mass spectrometry, *Env. Sci. & Tech.*, *42*(12), 4478-4485.

220 Bateman, A. P., et al. (2009), Time-resolved molecular characterization of limonene/ozone aerosol using
221 high-resolution electrospray ionization mass spectrometry, *Phys. Chem. Chem. Phys.*, *11*(36), 7931-7942.

222 Calvert, J. G., et al. (2000), *The Mechanisms of Atmospheric Oxidation of the Alkenes*, Oxford University
223 Press.

224 Capes, G., et al. (2009), Secondary organic aerosol from biogenic VOCs over West Africa during
225 AMMA, *Atmos. Chem. and Phys.*, *9*(12), 3841-3850.

226 Carlton, A. G., et al. (2007), Atmospheric oxalic acid and SOA production from glyoxal: Results of
227 aqueous photooxidation experiments, *Atmos. Env.*, *41*(35), 7588-7602.

228 Chen, Q., et al. (2009), Mass spectral characterization of submicron biogenic organic particles in the
229 Amazon Basin, *Geophys. Res. Lett.*, *36*(L20806), doi: 10.1029/2009GL039880.

230 de Gouw, J. A., et al. (2005), Budget of organic carbon in a polluted atmosphere: Results from the New
231 England Air Quality Study in 2002, *J. of Geophys. Res.*, *110*(D16).

232 DeCarlo, P. F., et al. (2006), Field-deployable, high-resolution, time-of-flight aerosol mass spectrometer,
233 *Anal. Chem.*, *78*(24), 8281-8289.

234 DeCarlo, P. F., et al. (2008), Fast airborne aerosol size and chemistry measurements above Mexico City
235 and Central Mexico during the MILAGRO campaign, *Atmos. Chem. and Phys.*, *8*(14), 4027-4048.

236 Heald, C. L., et al. (2005), A large organic aerosol source in the free troposphere missing from current
237 models, *Geophys. Res. Lett.*, *32*(18).

238 Heald, C. L., et al. (2006), Concentrations and sources of organic carbon aerosols in the free troposphere
239 over North America, *J. of Geophys. Res.*, *111*(D23).

240 Huffman, J. A., et al. (2009), Chemically-Resolved Volatility Measurements of Organic Aerosol from
241 Different Sources, *Env. Sci. & Tech.*, *43*(14), 5351-5357.

242 Johnson, D., et al. (2006), Simulating regional scale secondary organic aerosol formation during the
243 TORCH 2003 campaign in the southern UK, *Atmos. Chem. and Phys.*, *6*, 403-418.

244 Kalberer, M., et al. (2004), Identification of polymers as major components of atmospheric organic
245 aerosols, *Science*, *303*(5664), 1659-1662.

246 Kim, S., et al. (2003), Graphical method for analysis of ultrahigh-resolution broadband mass spectra of
247 natural organic matter, the van Krevelen diagram, *Anal. Chem.*, *75*(20), 5336-5344.

248 Kleinman, L. I., et al. (2008), The time evolution of aerosol composition over the Mexico City plateau,
249 *Atmos. Chem. and Phys.*, *8*(6), 1559-1575.

250 Kroll, J. H., et al. (2005), Secondary organic aerosol formation from isoprene photooxidation under high-
251 NO_x conditions, *Geophys. Res. Lett.*, *32*(18), doi:10.1029/2005GL023637.

252 Kroll, J. H., et al. (2009), Measurement of fragmentation and functionalization pathways in the
253 heterogeneous oxidation of oxidized organic aerosol, *Phys. Chem. Chem. Phys.*, *11*, 8005–8014.

254 Lim, Y. B., and P. J. Ziemann (2009), Chemistry of Secondary Organic Aerosol Formation from OH
255 Radical-Initiated Reactions of Linear, Branched, and Cyclic Alkanes in the Presence of NO_x, *Aer. Sci.*
256 *and Tech.*, *43*(6), 604-619.

257 Robinson, A. L., et al. (2007), Rethinking organic aerosols: Semivolatile emissions and photochemical
258 aging, *Science*, *315*(5816), 1259-1262.

259 Shilling, J. E., et al. (2009), Loading-dependent elemental composition of alpha-pinene SOA particles,
260 *Atmos. Chem. and Phys.*, *9*(3), 771-782.

261 Van Krevelen, D. W. (1950), Graphical-statistical method for the study of structure and reaction
262 processes of coal, *Fuel*, 269-284.

263 Volkamer, R., et al. (2006), Secondary organic aerosol formation from anthropogenic air pollution: Rapid
264 and higher than expected, *Geophys. Res. Lett.*, 33(17).

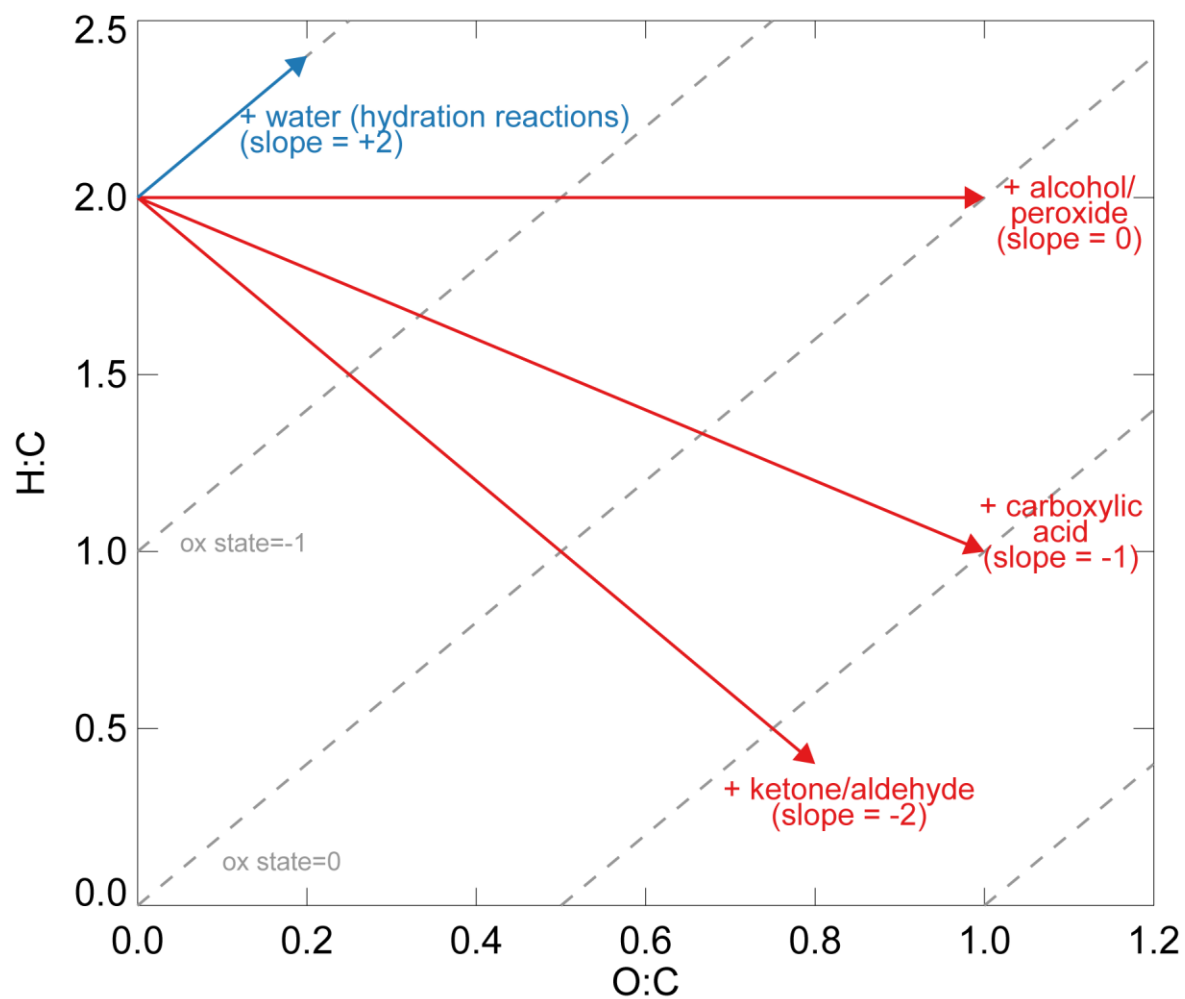
265 Volkamer, R., et al. (2009), Secondary Organic Aerosol Formation from Acetylene (C₂H₂): seed effect
266 on SOA yields due to organic photochemistry in the aerosol aqueous phase, *Atmos. Chem. and Phys.*,
267 9(6), 1907-1928.

268 Williams, B. J., et al. (2007), Chemical speciation of organic aerosol during the International Consortium
269 for Atmospheric Research on Transport and Transformation 2004: Results from in situ measurements, *J.*
270 *of Geophys. Res.*, 112(D10).

271 Zhang, Q., et al. (2007), Ubiquity and dominance of oxygenated species in organic aerosols in
272 anthropogenically-influenced Northern Hemisphere midlatitudes, *Geophys. Res. Lett.*, 34(L13801),
273 doi:10.1029/2007GL029979.

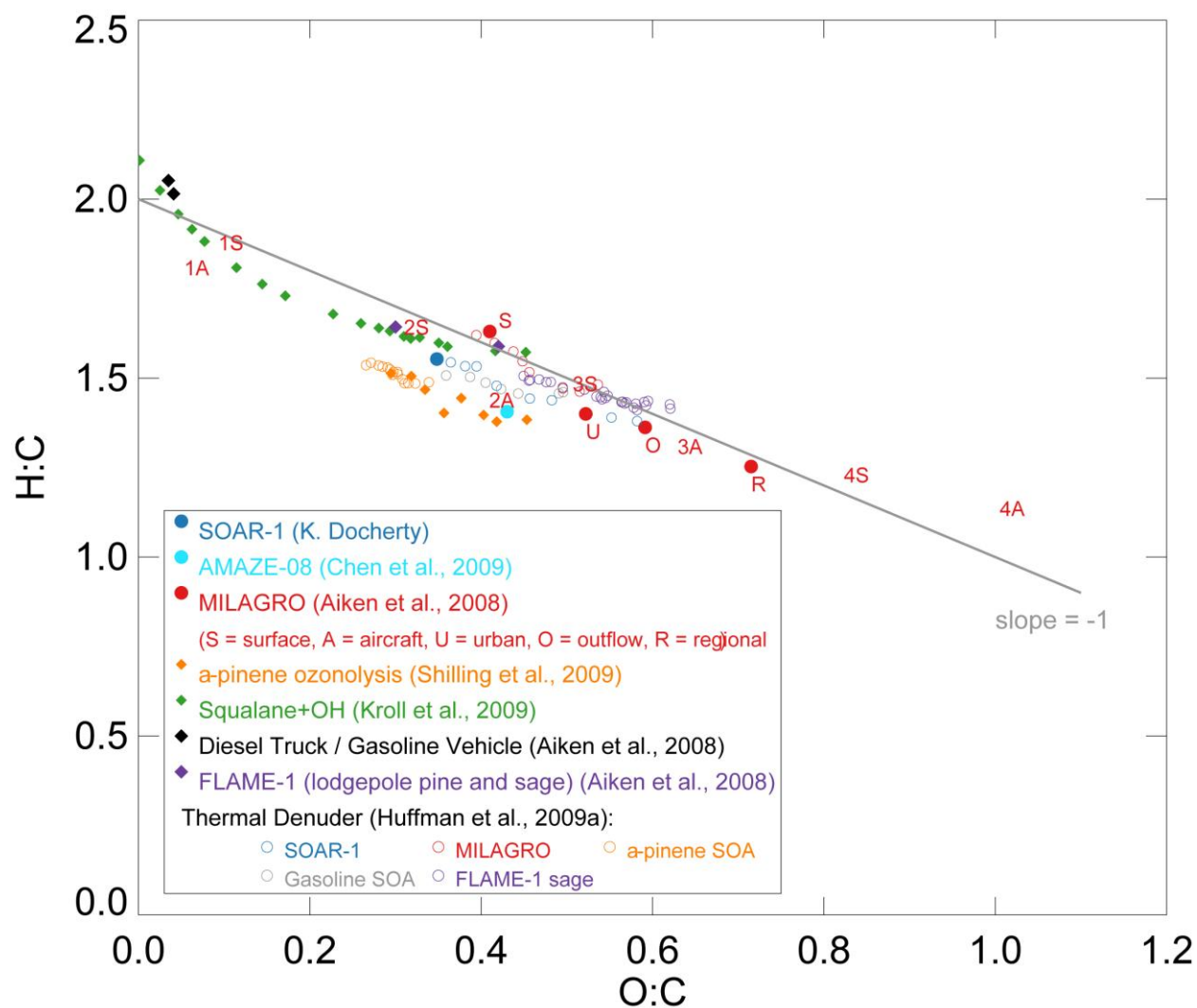
274

275

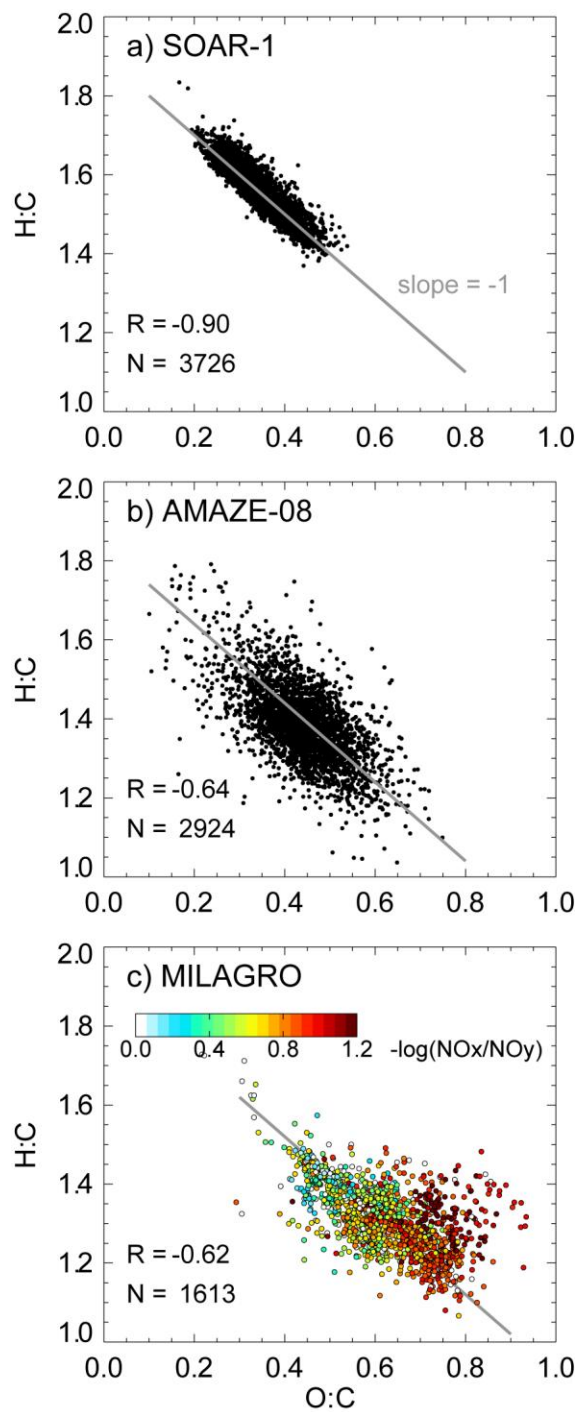


276

277 **Figure 1:** Van Krevelen diagram illustrating how functionalization reactions of organic species affect
 278 H:C and O:C from an arbitrary starting point. Each arrow corresponds to the addition of a particular
 279 functional group to an aliphatic (unfunctionalized) carbon. Lines of constant carbon oxidation state are
 280 shown in grey.



281
 282 **Figure 2:** Van Krevelen diagram of elemental ratios estimated from HR-AMS measurements of organic
 283 aerosol. These include mean observations from field studies (solid circles), lab studies (diamonds), and
 284 thermal denuder experiments (open circles). Also shown are the positive matrix factorization components
 285 of the MILAGRO observations (1=HOA, 2=BBOA, 3=OOA2, 4=OOA1) [Aiken *et al.*, 2008]. Line with -
 286 1 slope is illustrative and originates at O:C = 0 and H:C = 2, corresponding to an arbitrarily long acyclic
 287 alkane.



288

289 **Figure 3:** Van Krevelen diagrams of the elemental ratios of organic aerosol measured by AMS during a)
 290 the SOAR-1 campaign at Riverside, CA (5 minute average); b) the AMAZE-08 campaign in the Central
 291 Amazon Basin (5 minute average); c) the MILAGRO C-130 aircraft campaign over Mexico City (1
 292 minute average) colored by a photochemical clock, represented by the conversion of nitrogen oxides

293 (NO_x) to total reactive nitrogen (NO_y). Lines with -1 slope are illustrative. Correlation coefficient (R) and
294 number of observations (N) are shown. Low loadings increase the uncertainty in elemental analysis, thus
295 observations with OA loadings less than 0.3 μg/m³ are not shown.